Imaging Heterogeneously Distributed Photo-Active Traps in Perovskite Single Crystals

Haifeng Yuan, Elke Debroye, Eva Bladt, Gang Lu, Masoumeh Keshavarz, Kris P. F. Janssen, Maarten B. J. Roeffaers, Sara Bals, Edward H. Sargent,* and Johan Hofkens*

Organic–inorganic halide perovskites (OIHPs) have demonstrated outstanding energy conversion efficiency in solar cells and light-emitting devices. In spite of intensive developments in both materials and devices, electronic traps and defects that significantly affect their device properties remain under-investigated. Particularly, it remains challenging to identify and to resolve traps individually at the nanoscopic scale. Here, photo-active traps (PATs) are mapped over OIHP nanocrystal morphology of different crystallinity by means of correlative optical differential super-resolution localization microscopy (Δ-SRLM) and electron microscopy. Stochastic and monolithic photoluminescence intermittency due to individual PATs is observed on monocrystalline and polycrystalline OIHP nanocrystals. Δ-SRLM reveals a heterogeneous PAT distribution across nanocrystals and determines the PAT density to be 1.3×10^{14} and 8×10^{13} cm^{-3} for polycrystalline and for monocrystalline nanocrystals, respectively. The higher PAT density in polycrystalline nanocrystals is likely related to an increased defect density. Moreover, monocrystalline nanocrystals that are prepared in an oxygen- and moisture-free environment show a similar PAT density as that prepared at ambient conditions, excluding oxygen or moisture as chief causes of PATs. Hence, it is concluded that the PATs come from inherent structural defects in the material, which suggests that the PAT density can be reduced by improving crystalline quality of the material.

The rapid emergence of organic–inorganic halide perovskites (OIHPs) for optoelectronics applications, including photovoltaics,[1–7] light-emitting devices,[8–14] and photodetectors,[15–18] has drawn much research attention in recent years. Many efforts have been made in optimizing their macroscale device performance by improving material processing and device fabrication; however, many questions remain unanswered. Particularly, experimental investigations at a nanoscopic level are urgently required to deepen understanding of often-observed heterogeneous properties in polycrystalline OIHP films. Grain boundaries (GBs), the morphological gaps that define each crystal grain, are found to seclude photophysical properties of each crystal grain.[19] de Quilettes et al. recently reported inter-grain heterogeneity in photoluminescence (PL) intensity and decay times of micron-sized crystal grains in OIHP polycrystalline films.[19] Next to grain boundaries, crystal facets, local chemical composition, defects, and trap densities are recently found to all contribute to heterogeneity.[19–25] The recently reported migration of ionic and defect species driven by light or electric field and their influence on material properties provide further insight into the highly dynamic and complex nature of these materials.[22,26–34]

Dr. H. Yuan, Dr. E. Debroye, Dr. G. Lu, Dr. M. Keshavarz,
Dr. K. P. F. Janssen, Prof. J. Hofkens
Department of Chemistry
KU Leuven
Celestijnenlaan 200F, B-3001 Leuven, Belgium
E-mail: johan.hofkens@kuleuven.be
Dr. H. Yuan, Prof. E. H. Sargent
Department of Electrical and Computer Engineering
University of Toronto
10 King's College Road, Toronto, Ontario M5S 3G4, Canada
E-mail: ted.sargent@utoronto.ca
Dr. E. Bladt, Prof. S. Bals
EMAT
University of Antwerp
Groenenborgerlaan 171, 2020 Antwerp, Belgium

Dr. G. Lu
Key Laboratory of Flexible Electronics & Institute of Advanced
Materials
Nanjing Tech University
30 South Puzhu Road, 211816 Nanjing, China
Prof. M. B. J. Roeffaers
Centre for Surface Chemistry and Catalysis
KU Leuven
Celestijnenlaan 200F, B-3001 Leuven, Belgium
Prof. J. Hofkens
RIES
Hokkaido University
N20W10, Kita-Ward Sapporo 001-0020, Japan

Traps that directly interact with charge carriers are deterministic to the materials' optoelectrical properties in strikingly different ways.[35] On the one hand, the shallower hole traps associated with iodine interstitial defects are recently proposed in a theoretical work to extend charge carrier lifetimes, which is beneficial to the material's optoelectronic applications.[36] On the other hand, other traps, likely electron traps, result in energy loss by creating nonradiative recombination pathways for charge carriers, compromising the material's optoelectronic performance.[37] Thus far, analysis on traps in OIHP materials has been mostly carried out by bulk electrical and optical measurements, in which the overall trap densities on the order of $10^9 – 10^{10}$ cm^{-3} and $10^{15} – 10^{19}$ cm^{-3} are reported for bulk single crystals and polycrystalline films, respectively.[38–42] The bulk results are good indications for the overall material quality. Nonetheless, it remains challenging to resolve the spatial distribution of traps at the nanoscale and to distinguish the nonradiative traps from other types of traps, making it difficult to evaluate how the traps affect the charge carrier dynamics in the material on the nanometer scale.

Recent developments in single particle PL microscopy on colloidal OIHP nanocrystals make it possible to probe nonradiative traps in OIHP nanocrystals up to 200 nm ($10^2 – 10^8$ nm^3 in volume) by monitoring PL intermittency on well-isolated crystals.[43–47] Such an active trap efficiently quenches PL emission by generating efficient nonradiative recombination pathways for charge carriers, resulting in PL intermittency. Detailed analysis revealed power-low statistic of the PL intermittency, that can essentially be rationalized as trapping/detrapping processes.[44,45] Furthermore, the observed environment-dependency of PL intermittency suggests the presence of traps close to perovskite surface. Because these traps show a strong dependence on light illumination,[43,44] they will be referred to as photo-active traps (PATs) hereafter. PATs have a negative impact on the performance of photovoltaics and light-emitting devices and elimination of trap-assisted nonradiative recombination might therefore be an effective strategy toward more efficient OIHP applications. While recent studies imply that PATs might also be associated to structural defects,[44,48–50] their exact nature and origin remains largely elusive, hindering developments to specifically minimize PATs for improved OIHP applications.

Herein, we unravel the link between PATs and structural defects by resolving individual PATs in single nanocrystals using correlative optical differential super-resolution localization microscopy (Δ-SRLM), scanning electron microscopy (SEM), and high-angle annular dark field scanning transmission electron microscopy (HAADF-STEM). By fine-tuning the ligand-assisted synthesis, methylammonium lead iodide (MAPbI$_3$) single crystals of controlled morphology and crystallinity are prepared. Monolithic single-step PL intermittency are observed in both monocrystalline and polycrystalline MAPbI$_3$ single crystals up to several microns in size, showing that a single PAT can dictate the PL emission process of an entire single crystal of micrometer size, regardless to the presence of epitaxial domain boundaries. The finding here implies that epitaxial domain boundaries in a polycrystalline crystal have negligible influence on charge carrier diffusion in the micrometer range, providing fundamental insights for understanding the surprising fact that polycrystalline OHIP films

can support high conversion efficiencies. We here, for the first time, use Δ-SRLM to map the spatial distribution of PATs and show this distribution is correlated to particle morphology and crystallinity as revealed in SEM and HAADF-STEM. This allows visualization of PAT spatial density for nanocrystals of different morphology and crystallinity, namely, monocrystalline nanorods, monocrystalline nanoplates, and polycrystalline polyomino plates. While the PAT density does not vary notably in monocrystalline crystals of different morphology, the significantly higher PAT density found in polycrystalline nanocrystals indicates that PATs are related to structural defects.

In conventional SRLM, localization-fitting algorithms are applied onto the stochastically switching single-emitter PL signals between a bright and a dark state, so that the emission center position can be determined. The technique holds for a single active emitter within a diffraction-limited volume, which can be identified by the signature of single-step PL intermittency or photobleaching. Building on sufficient photon statistics, the optical resolution can be improved down to a few nanometers.[51,52] Thanks to the PL intermittency of OIHP nanocrystals, optical SRLM can be applied to identify the well-isolated nanocrystal containing PATs with a spatial resolution beyond the optical diffraction limit.[44,45] Direct application of conventional SRLM on densely packed perovskite nanocrystals in a film is, however, not straightforward. Particularly, perovskite PL possesses long-lived bright states and low occurrences of PL intermittency, leading to a strong and almost constant PL background in a film sample or a densely-packed cluster of nanocrystals. To apply the method to clusters of perovskite nanocrystals that recreate films used in devices, here we adapt the localization-fitting procedure using PL differences between consecutive images, namely, differential SRLM (Δ-SRLM), to map the PL intermittency events caused by PATs. Δ-SRLM fitting is carried out on the intensity differential images calculated from video data of 10 000 frames (frame time 50 ms) of each sample area. Briefly, every frame of the PL movie (I_{n+1}) is subtracted by its previous frame (I_n), so that the intensity different image (ΔI_n) can be generated and can be described by $\Delta I_n = I_{n+1} - I_n$. The differential images thus reflect the PL intensity changes during intermittency events. Applying 2D-Gaussian fitting on the intensity differential images, one can identify and localize the PL intermittency events, even in the presence of a high constant background.

Monocrystalline and polycrystalline nanocrystals of several hundred nanometers are prepared by a ligand-assisted solution synthesis method, modified from a previously reported method.[44,53] To exclude surface effects,[19,39,44] tri-*n*-octylphosphine oxide is used in the synthesis for surface passivation.[54] The surface passivation eliminates the surface traps that are responsible for the majority of PL blinking events in earlier reports, yielding an extended PL decay time of 118 ns that is almost doubled from the nonpassivated nanorods.[44] In addition, the surface passivation isolates perovskite from direct interaction with oxygen and moisture in air, thus providing enhanced stability during optical measurements, making it possible to acquire sufficient long movies, hence improving statistics for locating PATs by Δ-SRLM. **Figure 1** shows typical SEM images of the synthesized nanorods and nanoplates. HAADF-STEM reveals the monocrystalline nature of the nanorods and
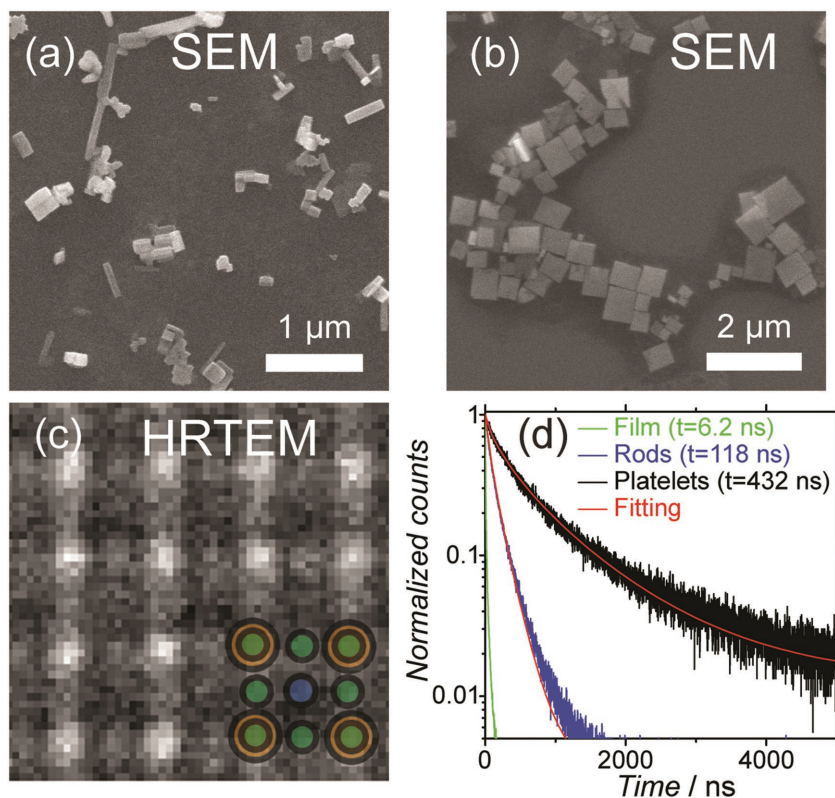
Figure 1. a) Typical SEM image of MAPbI$_3$ nanorods. b) SEM image of MAPbI$_3$ nanoplates. c) HAADF-STEM image on a single nanoplate. To minimize the material damage by electron beams, a small electron dose was used. A template-based algorithm was applied to enhance the signal-to-noise ratio. d) PL decay curves measured on a polycrystalline OIHP film, monocrystalline nanorods, and nanoplates. The red solid lines represent fittings using stretched exponential functions. The characteristic decay times are 6.2, 118, and 432 ns for the film, nanorods, and nanoplates, respectively.

PAT is screened by the photo-generated charges in a nanocrystal whose dimensions are much less than the average charge diffusion length. Even though charge mobility and charge diffusion length can vary between different sample preparation methods,[56] polycrystalline grains in thin films can result in charge diffusion lengths of a few hundred nanometers.[56–58] Here we use reported charge mobility in large single crystals MAPbI$_3$[59] and the measured PL decay times to estimate charge diffusion lengths to be 4.3 µm in nanorods (118 ns) and 8.2 µm in nanoplates (432 ns). Both values are far larger than the crystal dimensions here, resulting in the observed monolithic PL intermittency behavior.

Monolithic PL intermittency is also found in polycrystalline crystals. When we deliberately reduce the capping ligand concentration in synthesis, we see polyomino-shaped nanocrystals (see experimental section in the Supporting Information). In contrast with the regular rods and plates, the polyomino-shaped crystals are polycrystalline, as revealed in HAADF-STEM measurements (Figure S2, Supporting Information). Though it is difficult to achieve uniform polycrystalline nanocrystals in the synthesis condition used, polycrystalline crystals can be distinguished from their monocrystalline counterparts by their distinct morphology revealed by SEM. The SEM image and PL images of such a polycrystalline crystal (outlined with orange solid lines) are given in **Figure 3**a–c. This crystal shows monolithic PL intermittency under the identical experimental condition as used for monocrystalline nanocrystals. Both its bright state (Figure 3b) and dim state (Figure 3c) show homogeneous PL intensity across the entire structure. PL intensity time traces at two spots separated by 1 µm show a strong correlation (Figure 3d–e), similar as that observed on their monocrystalline counterparts. The presence of polycrystalline domain boundaries (PDBs) in this case does not have an apparent influence on the monolithic PL intermittency behavior, even though a higher defect density is expected for polycrystalline nanocrystals due to PDBs. This observation indicates that PDBs have limited influence on the charge dynamics at 1 µm's length scale. In other words, the charge mobility within 1 µm's range is not confined by PDBs, which possibly results from epitaxial growth of the polycrystals, similar as that reported in quantum dots systems.[60–63] This finding here coincides with the fact that polycrystalline films of several hundred nanometers show excellent charge mobility for solar cell applications.[57,59]

GBs, on the other hand, are found to isolate PL intermittency to individual crystals within a densely packed cluster. Each crystal grain shows independent and stochastic PL intermittency even though they are in close contact with each other. **Figure 4**a,b shows the SEM image and the PL image of a five-crystal cluster. By consecutively subtracting each frame by its

nanoplates. The observed crystal lattice parameter of 6.4 Å is in agreement with that of the cubic phase MAPbI$_3$ ($a = 6.455$ Å).[55] MAPbI$_3$ nanorods and nanoplates show PL decay times of 118 and 432 ns, respectively. PL decay curves of nanorods and nanoplates, fit with stretched exponential functions, are shown in Figure 1d.

Figure 2a–c presents PL images and the SEM image on a single nanorod of 1800 nm in length and 100 nm in width. The nanorod shows PL intermittency between a bright state (Figure 2a) and a dim state (Figure 2b) with time. Interestingly, PL intensity across the entire rod shows a homogeneous intensity level throughout the measurement regardless to the bright or dim state, suggesting monolithic PL intermittency behavior. To further demonstrate this point, PL intensity time traces (Figure 2d) are extracted for two regions at opposing ends of the nanorod as indicated by black and red squares in Figure 2a–c. PL intensities at these two ends show an almost unity correlation coefficient (0.972, Figure 2e). The distance between the two spots largely exceeds the diffraction limit, such that PL crosstalk can be safely excluded. The observed single-step and monolithic PL intermittency observed on OIHP nanocrystals is likely due to a single PAT inside the nanorod.

The ability of a single PAT to control the PL intermittency of a nanocrystal is associated with long charge diffusion length: the

**ADVANCED
SCIENCE NEWS**

www.advancedsciencenews.com
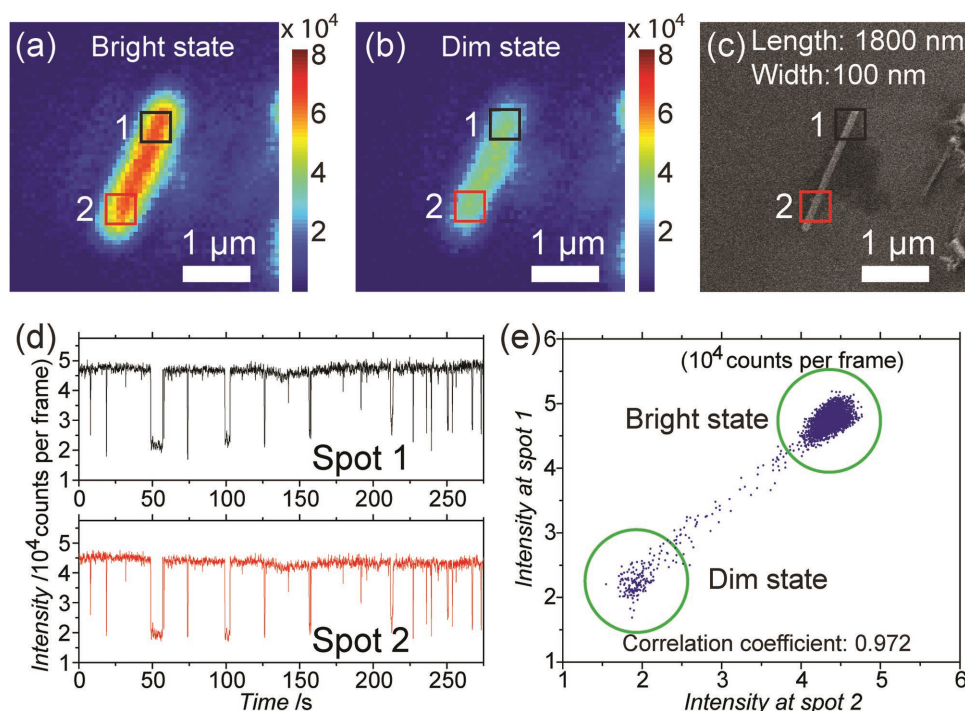
**ADVANCED
MATERIALS**

www.advmat.de

Figure 2. a,b) PL image of a monocrystalline OIHP nanorods of 1800 nm length in its bright state and dim state, respectively. c) SEM image of the same nanorod shown in (a) and (b). Volume is approximately 7.2×10^6 nm³. d) PL intensity time traces recorded at the two ends of the nanorod. e) Scattered plot of PL intensities at the two ends of the nanorod shows a strong correlation. The correlation coefficient is 0.972.

previous frame, we can visualize each PL intermittency event by its intensity difference between the bright and the dim states, as demonstrated in Figure 4c–f. Except the nanocrystal labeled as "P2" which shows a steady and weak PL emission, all

the remaining four nanocrystals can be identified respectively in their differential PL images in Figure 4c–f. Because of the monolithic PL intermittency, there differential images closely resemble the particle morphology as revealed in the SEM
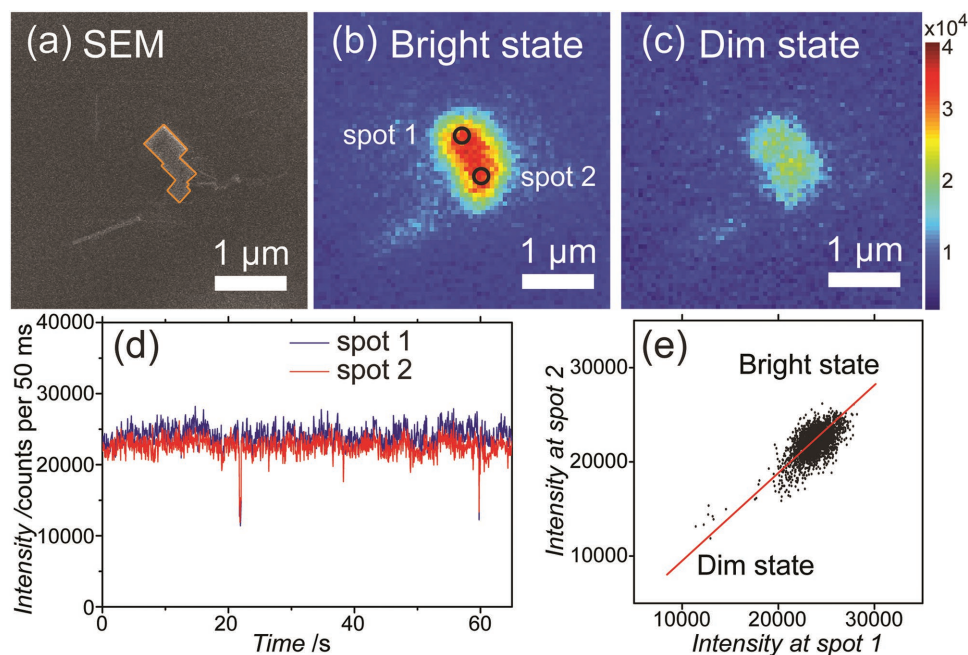

Figure 3. a) SEM image of a polycrystalline nanocrystal. The volume is about 9×10^6 nm³. b,c) PL image of the polycrystalline OIHP nanocrystal in its bright state and dim state, respectively. d) PL intensity time traces recorded at the two ends of the crystal. e) Scatter plot of PL intensities at the two ends of the crystal shows a strong correlation.
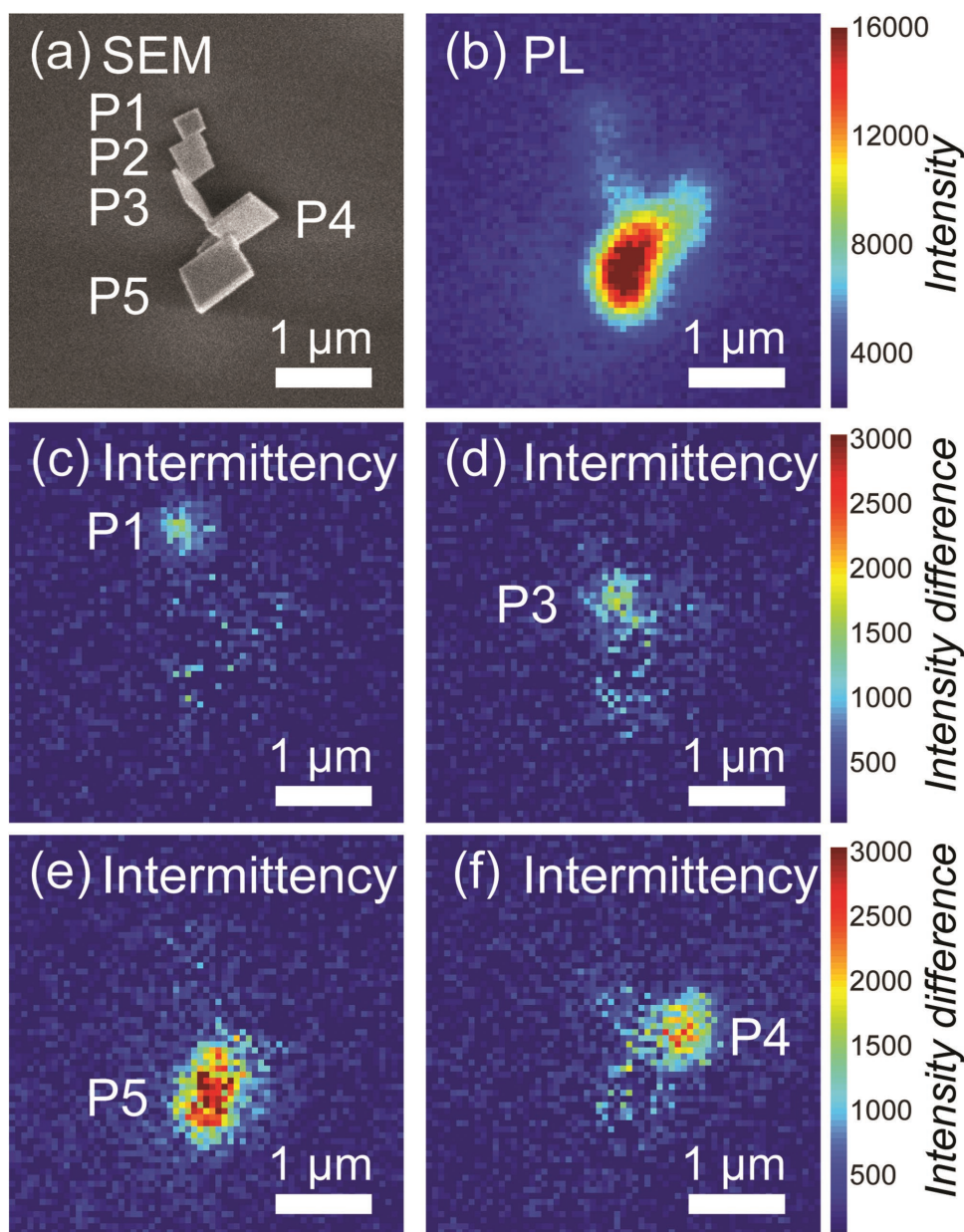
**ADVANCED
SCIENCE NEWS**

www.advancedsciencenews.com

**ADVANCED
MATERIALS**

www.advmat.de

Figure 4. a) SEM image of a cluster of five plate-like nanocrystals. b) PL image of the same nanocrystal cluster in (a). c–f) Differential PL intensity images during stochastic intermittency of each individual nanocrystal.

image. The observed independent and stochastic PL intermittency is crucial for later Δ-SRLM investigation, vide infra.

It should be noted that the distribution of PATs is heterogeneous: nanocrystals with different numbers of PATs can be found in our experiments. For instance, P2 in Figure 4 does not show any PL intermittency, indicating absence of a PAT within the experiment window. Many nanocrystals show single-step PL intermittency with constant intensity levels in their bright and dim states, indicating the presence of one single PAT. Moreover, we find occasionally (less than 5%) single crystals showing multiple-step PL intermittency, as illustrated in **Figure 5**. A plate-like nanocrystal with lateral dimensions of 600×440 nm^2 (Figure 5a) shows multiple distinct intensity levels in its PL

intensity time trace (Figure 5b), indicating the existence of two independent PATs. The two PATs show different PL intermittency step amplitudes. One PAT quenched the nanocrystal PL from 0.9 to 0.3, showing an intermittency amplitude of 0.6 in intermittency event A (Figure 5b). The other PAT results in an intermittency step from 0.9 to 0.45 with amplitude of 0.45 in another intermittency event B (Figure 5b). When both PATs are active, the nanocrystal PL is quenched entirely. The observation shows the capability of Δ-SRLM to identify multiple traps in a single crystal.

We offer two possible explanations for the different PL intermittency amplitudes. PATs may have different trap depths, thus having different efficiency in charge trapping.
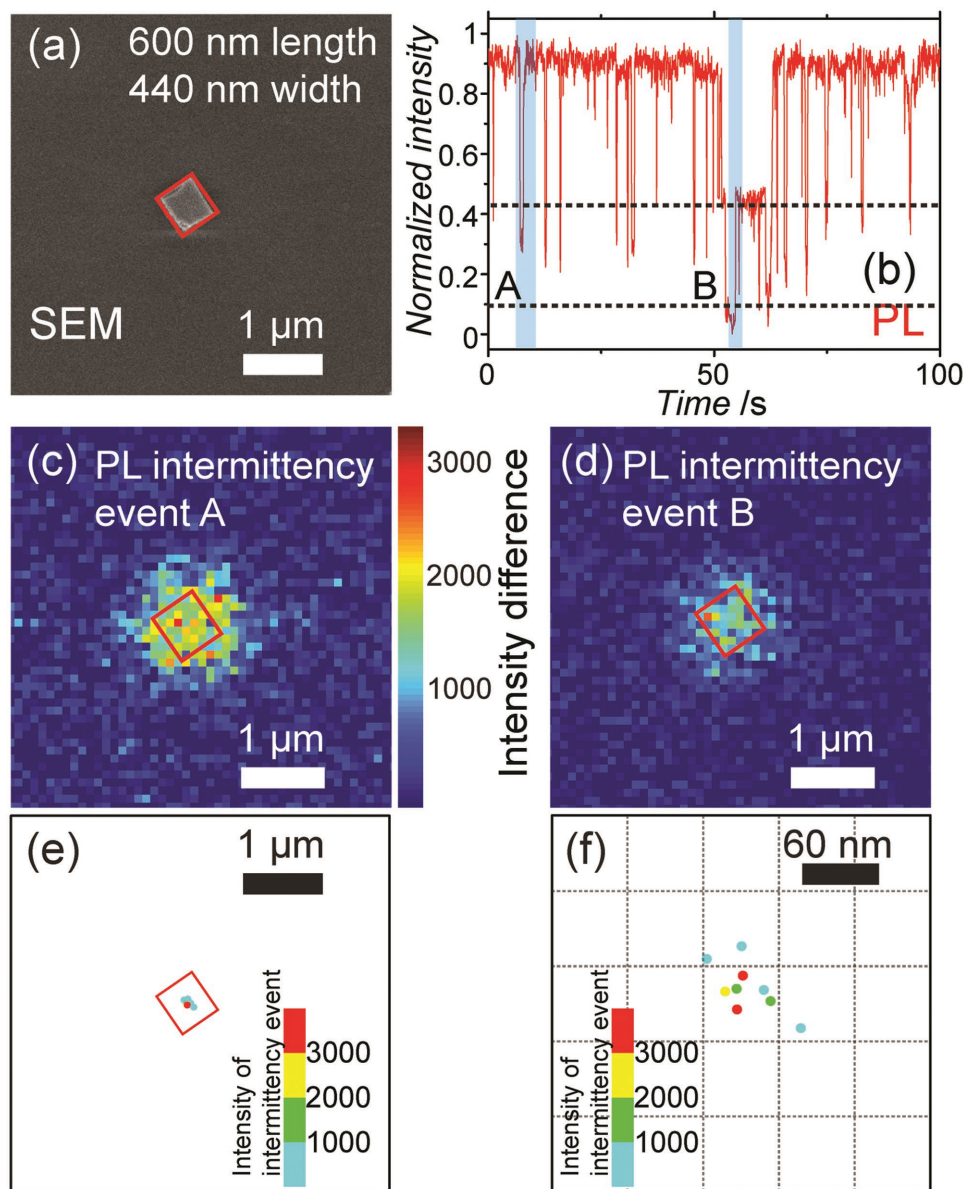
**ADVANCED
SCIENCE NEWS**

www.advancedsciencenews.com

**ADVANCED
MATERIALS**

www.advmat.de

Figure 5. a) SEM image of a plate-like nanocrystals. The lateral dimension is 600 nm × 440 nm. b) PL intensity time trace of the nanocrystal under constant illumination. Two intermittency intensity levels, highlighted with dashed lines, can be recognized. Light blue color is used to highlight two intermittency events of different amplitudes. c,d) PL intensity differential images of the intermittency events A and B, which are highlighted in (b). e) Reconstructed super-resolution map of the intermittency events. The red solid square outlines the morphology of the nanocrystal. The color bar represents the amplitude in each intermittency event. f) Zoom-in map of the intermittency events. The color bar represents the amplitude in each intermittency event.

On the other hand, the two PATs are very likely to locate at different positions in the crystal, thus may screen different surroundings or charge carrier densities. However, both PATs induce monolithic PL intermittency and screen the charge carriers generated across the entire nanocrystal, evident from their identical PL intensity differential images at different intermittency events (Figure 5c,d) and the overlapped localization results of intermittency events with different amplitudes (Figure 5e,f). Although the exact position of PATs cannot be determined in this case, the chance for two PATs to locate close to each other is very low due to the low average PAT

density (8.3×10^{13} cm^{-3}, which corresponds to 0.8 PAT in this nanocrystal).

The independent and stochastic PL intermittency of individual nanocrystals allows us to apply Δ-SRLM to map PATs at a high spatial resolution. Though a precise localization of a PAT is not feasible due to monolithic PL intermittency of an entire nanocrystal of several hundred nanometers.[38,43,47,64] **Figure 6**a,b shows a cluster of rod-like OIHP nanocrystals (approximately 100 nm in length and 40 nm in width) and its PL image. By applying localization fitting, we reconstruct a super-resolution map of PATs in Figure 6c. Though all parts
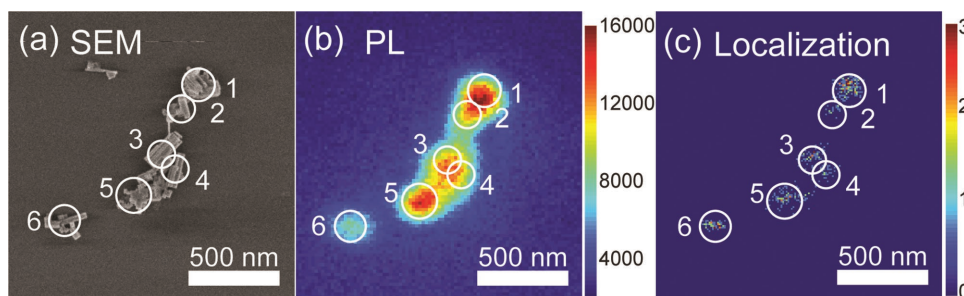
ADVANCED
SCIENCE NEWS
www.advancedsciencenews.com

ADVANCED
MATERIALS
www.advmat.de

Figure 6. a) SEM image on a cluster of rod-like OIHP nanocrystals. b) PL image on the cluster in (a). c) Reconstructed localization image on PL intermittency events of the cluster.

of the cluster appear luminescent in the diffraction-limited PL image (Figure 6b), only six active PL intermittency sites can be identified in the super-resolution mapping in Figure 6c. These PL intermittency sites correspond to nanocrystals with active PATs. The located PATs are highlighted with white solid cycles in Figure 6a–c. Dividing the number of PATs by the total volume of the cluster, we can determine the overall PAT density in each sample. The volume of the luster can be estimated using the morphology data acquired in SEM and height information revealed in atomic force microscopy (average thickness 32 nm). The PAT density is calculated for more than five clusters, each contains dozens of nanocrystals. We find that the standard deviation of the PAT density estimated for each cluster is within 10%. The mean value from multiple clusters was taken for each sample. In this way, we estimate the average PAT density in the monocrystalline nanorod sample, in the monocrystalline nanoplate sample and in the polycrystalline nanoplate sample to be 8.6×10^{13}, 8.3×10^{13}, and 1.3×10^{14} cm^{-3}, respectively. These values are 10^4 times higher than those determined by the Hall effect and current–voltage measurements (10^9–10^{10} cm^{-3}) for large single crystals,[38] but are 10^2 times lower than that revealed in time-resolved PL measurements (5×10^{16} cm^{-3} in bulk and 1.6×10^{17} cm^{-3} at surfaces).[14,39]

The difference in trap densities between the values determined in this work and the literature values may come from several factors. (i) Different sample processing methods could influence the material properties.[20] (ii) Even though the nanocrystals are surface-passivated with ligands, the very large surface to volume ratio of nanocrystals may readily lead to higher trap densities in nanocrystals. (iii) Different experimental techniques (electrical and optical) could be sensitive to different types of traps/defects because of their different nature. For instance, the optical method described here is based on the PL intermittency phenomena to probe PATs that generate nonradiative recombination pathways instead of traps of other nature.

The comparable PAT density values found in monocrystalline crystals, despite of the different morphology, excludes morphology factors to contribute to PATs in our experiments. The significantly higher PAT density observed in polycrystalline nanocrystals, on the other hand, indicates PATs to be linked with structural defects. It is also noteworthy that a similar PAT density of 8×10^{13} cm^{-3} is found in monocrystalline nanocrystals prepared in an oxygen- and moisture-free environment ($O_2 < 0.1$ ppm, $H_2O < 0.1$ ppm), indicating that oxygen or moisture during nanocrystal synthesis is unlikely to relate with

PATs. Therefore, we conclude that PATs are from inherent structural defects in the perovskite crystals.

Inherent structural defects in OIHP are present in many forms, including vacancies, interstitials, antisites, edge dislocations, and polycrystalline grain boundaries, and have very different formation energies.[35] Nonetheless, vacancies and interstitials in MAPbI$_3$ create only shallow traps.[65] Deep traps that mediate nonradiative recombination can come from structural defects such as Pb-I antisites,[50,66] MA-I antisites[50] and often require a high formation energy. We thus speculate that the energetically less stable polycrystalline boundaries can facilitate deep trap formation under light illumination, likely associated with ion dynamics. It is noteworthy that the major species of the deep traps can vary depending on the conditions used for material preparation.[50,66] We thus speculate that PATs or deep traps may be reduced by management of iodine content, since both the deep traps involves antisites by iodine ions. A very recent work employing this strategy has demonstrate power conversion efficiency of 22.1% in perovskite solar cells.[67] During the revision of this work, Li et al. reported on iodine migration and iodine vapor to quench PL of polycrystalline films, suggesting the important role of iodine in influencing PL emission properties of perovskite materials.[68]

In conclusion, different from previous reports, we have demonstrated Δ-SLRM on PATs in surface passivated MAPbI$_3$ crystals, bot mono- and poly-crystalline in nature, by contrast of PL intermittency. We find that stochastic and monolithic PL intermittency can be observed on crystals ranging from tens of nanometers up to microns in size. Moreover, this monolithic PL intermittency of polycrystalline crystals indicates that the charge dynamics is not sensitive to epitaxial polycrystalline domain boundaries up to at least a micron. This finding aligns with the fact that polycrystalline perovskite films with (sub) micron grain sizes and a few hundred-nanometer thicknesses can deliver high power conversion efficiency in photovoltaic devices. We furthermore show that the distribution of PATs is highly heterogeneous at the nanoscale and can vary from crystal to crystal. We further determine the PAT density to be about 8×10^{13} cm^{-3} for monocrystals and 1.3×10^{14} cm^{-3} for polycrystals. The higher PAT density found in polycrystals indicates PATs to be related to inherent structural defects. A detailed comparison between previous work and the data reported here is presented in table form in supporting info. The results here suggest eliminating PATs to improve optoelectronic performance of perovskite devices by improving the crystallinity of OIHP materials. The work here paves the way to apply super-resolution microscopy

**ADVANCED
SCIENCE NEWS**
www.advancedsciencenews.com

**ADVANCED
MATERIALS**
www.advmat.de

to study detailed properties of OIHP materials and can be potentially extended to other optoelectronic nanomaterials. The optical method demonstrated here can potentially be applied to monitor PATs in working optoelectric devices, this way gaining deeper insights at the nanoscopic/mesoscopic scale.

Supporting Information

Supporting Information is available from the Wiley Online Library or from the author.

Conflict of Interest

The authors declare no conflict of interest.

Keywords

defects, lead iodide perovskite nanocrystals, photo-active traps, photoluminescence, super-resolution optical microscopy

[1] M. Saliba, S. Orlandi, T. Matsui, S. Aghazada, M. Cavazzini, J. P. Correa-Baena, P. Gao, R. Scopelliti, E. Mosconi, K. H. Dahmen, F. De Angelis, A. Abate, A. Hagfeldt, G. Pozzi, M. Grätzel, M. K. A. Nazeeruddin, *Nat. Energy* **2016**, *1*, 15017.

[2] M. Liu, M. B. Johnston, H. J. Snaith, *Nature* **2013**, *501*, 395.

[3] N. K. Noel, S. D. Stranks, A. Abate, C. Wehrenfennig, S. Guarnera, A. A. Haghighirad, A. Sadhanala, G. E. Eperon, S. K. Pathak, M. B. Johnston, A. Petrozza, L. M. Herz, H. J. Snaith, *Energy Environ. Sci.* **2014**, *7*, 3061.

[4] W. Nie, H. Tsai, R. Asadpour, J. C. Blancon, A. J. Neukirch, G. Gupta, J. J. Crochet, M. Chhowalla, S. Tretiak, M. A. Alam, H. L. Wang, A. D. Mohite, *Science* **2015**, *347*, 522.

[5] H. Tsai, W. Nie, J. C. Blancon, C. C. Stoumpos, R. Asadpour, B. Harutyunyan, A. J. Neukirch, R. Verduzco, J. J. Crochet, S. Tretiak, L. Pedesseau, J. Even, M. A. Alam, G. Gupta, J. Lou, P. M. Ajayan, M. J. Bedzyk, M. G. Kanatzidis, A. D. Mohite, *Nature* **2016**, *536*, 312.

[6] N. G. Park, *Mater. Today* **2015**, *18*, 65.

[7] T. C. Sum, N. Mathews, *Energy Environ. Sci.* **2014**, *7*, 2518.

[8] X. Y. Chin, D. Cortecchia, J. Yin, A. Bruno, C. Soci, *Nat. Commun.* **2015**, *6*, 7383.

[9] S. A. Veldhuis, P. P. Boix, N. Yantara, M. Li, T. C. Sum, N. Mathews, S. G. Mhaisalkar, *Adv. Mater.* **2016**, *28*, 6804.

[10] J. Xing, F. Yan, Y. Zhao, S. Chen, H. Yu, Q. Zhang, R. Zeng, H. V. Demir, X. Sun, A. Huan, Q. Xiong, *ACS Nano* **2016**, *10*, 6623.

[11] M. Yuan, L. N. Quan, R. Comin, G. Walters, R. Sabatini, O. Voznyy, S. Hoogland, Y. Zhao, E. M. Beauregard, P. Kanjanaboos, Z. Lu, D. H. Kim, E. H. Sargent, *Nat. Nanotechnol.* **2016**, *11*, 872.

[12] N. Wang, L. Cheng, R. Ge, S. Zhang, Y. Miao, W. Zou, C. Yi, Y. Sun, Y. Cao, R. Yang, Y. Wei, Q. Guo, Y. Ke, M. Yu, Y. Jin, Y. Liu, Q. Ding, D. Di, L. Yang, G. Xing, H. Tian, C. Jin, F. Gao, R. H. Friend, J. Wang, W. Huang, *Nat. Photonics* **2016**, *10*, 699.

[13] H. Zhu, Y. Fu, R. Meng, X. Wu, Z. Gong, Q. Ding, M. V. Gustafsson, M. T. Trinh, S. Jin, X. Y. Zhu, *Nat. Mater.* **2015**, *14*, 636.

[14] G. Xing, N. Mathews, S. S. Lim, N. Yantara, X. Liu, D. Sabba, M. Grätzel, S. Mhaisalkar, T. C. Sum, *Nat. Mater.* **2014**, *13*, 476.

[15] H. Deng, X. Yang, D. Dong, B. Li, D. Yang, S. Yuan, K. Qiao, Y. B. Cheng, J. Tang, H. Song, *Nano Lett.* **2015**, *15*, 7963.

[16] Y. Fang, Q. Dong, Y. Shao, Y. Yuan, J. Huang, *Nat. Photonics* **2015**, *9*, 679.

[17] M. I. Saidaminov, V. Adinolfi, R. Comin, A. L. Abdelhady, W. Peng, I. Dursun, M. Yuan, S. Hoogland, E. H. Sargent, O. M. Bakr, *Nat. Commun.* **2015**, *6*, 8724.

[18] V. Adinolfi, O. Ouellette, M. I. Saidaminov, G. Walters, A. L. Abdelhady, O. M. Bakr, E. H. Sargent, *Adv. Mater.* **2016**, *28*, 7264.

[19] D. W. de Quilettes, S. M. Vorpahl, S. D. Stranks, H. Nagaoka, G. E. Eperon, M. E. Ziffer, H. J. Snaith, D. S. Ginger, *Science* **2015**, *348*, 683.

[20] A. Sharenko, M. F. Toney, *J. Am. Chem. Soc.* **2016**, *138*, 463.

[21] O. Hentz, Z. Zhao, S. Gradecak, *Nano Lett.* **2016**, *16*, 1485.

[22] H. Yuan, E. Debroye, K. Janssen, H. Naiki, C. Steuwe, G. Lu, M. Moris, E. Orgiu, H. Uji-i, F. De Schryver, P. Samorì, J. Hofkens, M. Roeffaers, *J. Phys. Chem. Lett.* **2016**, *7*, 561.

[23] S. Y. Leblebici, L. Leppert, Y. Li, S. E. Reyes-Lillo, S. Wickenburg, E. Wong, J. Lee, M. Melli, D. Ziegler, D. K. Angell, D. F. Ogletree, P. D. Ashby, F. M. Toma, J. B. Neaton, I. D. Sharp, A. Weber-Bargioni, *Nat. Energy* **2016**, *1*, 16093.

[24] C. G. Bischak, E. M. Sanehira, J. T. Precht, J. M. Luther, N. S. Ginsberg, *Nano Lett.* **2015**, *15*, 4799.

[25] S. Draguta, S. Thakur, Y. V. Morozov, Y. Wang, J. S. Manser, P. V. Kamat, M. Kuno, *J. Phys. Chem. Lett.* **2016**, *7*, 715.

[26] J. M. Azpiroz, E. Mosconi, J. Bisquert, F. De Angelis, *Energy Environ. Sci.* **2015**, *8*, 2118.

[27] C. Eames, J. M. Frost, P. R. F. Barnes, B. C. O'Regan, A. Walsh, M. S. Islam, *Nat. Commun.* **2015**, *6*, 7497.

[28] Y. Shao, Y. Fang, T. Li, Q. Wang, Q. Dong, Y. Deng, Y. Yuan, H. Wei, M. Wang, A. Gruverman, J. Shield, J. Huang, *Energy Environ. Sci.* **2016**, *9*, 1752.

[29] C. Li, S. Tscheuschner, F. Paulus, P. E. Hopkinson, J. Kießling, A. Köhler, Y. Vaynzof, S. Huettner, *Adv. Mater.* **2016**, *28*, 2446.

[30] D. W. deQuilettes, W. Zhang, V. M. Burlakov, D. J. Graham, T. Leijtens, A. Osherov, V. Bulovic, H. J. Snaith, D. S. Ginger, S. D. Stranks, *Nat. Commun.* **2016**, *7*, 11683.

[31] S. Meloni, T. Moehl, W. Tress, M. Franckevicius, M. Saliba, Y. H. Lee, P. Gao, M. K. Nazeeruddin, S. M. Zakeeruddin, U. Rothlisberger, M. Grätzel, *Nat. Commun.* **2016**, *7*, 10334.

[32] Z. Xiao, Y. Yuan, Y. Shao, Q. Wang, Q. Dong, C. Bi, P. Sharma, A. Gruverman, J. Huang, *Nat. Mater.* **2015**, *14*, 193.

[33] S. J. Yoon, M. Kuno, P. V. Kamat, *ACS Energy Lett.* **2017**, *2*, 1507.

**ADVANCED
SCIENCE NEWS**

www.advancedsciencenews.com

**ADVANCED
MATERIALS**

www.advmat.de

[34] W. Zhou, Y. Zhao, X. Zhou, R. Fu, Q. Li, Y. Zhao, K. Liu, D. Yu, Q. Zhao, *J. Phys. Chem. Lett.* **2017**, 4122.

[35] J. M. Ball, A. Petrozza, *Nat. Energy* **2016**, *1*, 16149.

[36] W. Li, J. Liu, F. Q. Bai, H. X. Zhang, O. V. Prezhdo, *ACS Energy Lett.* **2017**, *2*, 1270.

[37] G. J. A. H. Wetzelaer, M. Scheepers, A. M. Sempere, C. Momblona, J. Ávila, H. J. Bolink, *Adv. Mater.* **2015**, *27*, 1837.

[38] D. Shi, V. Adinolfi, R. Comin, M. Yuan, E. Alarousu, A. Buin, Y. Chen, S. Hoogland, A. Rothenberger, K. Katsiev, Y. Losovyj, X. Zhang, P. A. Dowben, O. F. Mohammed, E. H. Sargent, O. M. Bakr, *Science* **2015**, *347*, 519.

[39] B. Wu, H. T. Nguyen, Z. Ku, G. Han, D. Giovanni, N. Mathews, H. J. Fan, T. C. Sum, *Adv. Energy Mater.* **2016**, *6*, 1600551.

[40] J. A. Koza, J. C. Hill, A. C. Demster, J. A. Switzer, *Chem. Mater.* **2016**, *28*, 399.

[41] T. M. Brenner, D. A. Egger, L. Kronik, G. Hodes, D. Cahen, *Nat. Rev. Mater.* **2016**, *1*, 15007.

[42] G. Han, T. M. Koh, S. S. Lim, T. W. Goh, X. Guo, S. W. Leow, R. Begum, T. C. Sum, N. Mathews, S. Mhaisalkar, *ACS Appl. Mater. Interfaces* **2017**, *9*, 21292.

[43] Y. Tian, A. Merdasa, M. Peter, M. Abdellah, K. Zheng, C. S. Ponseca, T. Pullerits, A. Yartsev, V. Sundström, I. G. Scheblykin, *Nano Lett.* **2015**, *15*, 1603.

[44] H. Yuan, E. Debroye, G. Caliandro, K. P. F. Janssen, J. van Loon, C. E. A. Kirschhock, J. A. Martens, J. Hofkens, M. B. J. Roeffaers, *ACS Omega* **2016**, *1*, 148.

[45] A. Merdasa, Y. Tian, R. Camacho, A. Dobrovolsky, E. Debroye, E. L. Unger, J. Hofkens, V. Sundström, I. G. Scheblykin, *ACS Nano* **2017**, *11*, 5391.

[46] B. A. Rosales, M. P. Hanrahan, B. W. Boote, A. J. Rossini, E. A. Smith, J. Vela, *ACS Energy Lett.* **2017**, *2*, 906.

[47] F. Zhu, L. Men, Y. Guo, Q. Zhu, U. Bhattacharjee, P. M. Goodwin, J. W. Petrich, E. A. Smith, J. Vela, *ACS Nano* **2015**, *9*, 2948.

[48] M. Lorenzon, L. Sortino, Q. Akkerman, S. Accornero, J. Pedrini, M. Prato, V. Pinchetti, F. Meinardi, L. Manna, S. Brovelli, *Nano Lett.* **2017**, *17*, 3844.

[49] H. Uratani, K. Yamashita, *J. Phys. Chem. Lett.* **2017**, *8*, 742.

[50] S. Heo, G. Seo, Y. Lee, D. Lee, M. Seol, J. Lee, J. B. Park, K. Kim, D. J. Yun, Y. S. Kim, J. K. Shin, T. K. Ahn, M. K. Nazeeruddin, *Energy Environ. Sci.* **2017**, *10*, 1128.

[51] B. Huang, M. Bates, X. W. Zhuang, *Annu. Rev. Biochem.* **2009**, *78*, 993.

[52] D. Wöll, C. Flors, *Small Methods* **2017**, *1*, 1700191.

[53] E. Debroye, H. Yuan, E. Bladt, W. Baekelant, M. Van der Auweraer, J. Hofkens, S. Bals, M. B. J. Roeffaers, *ChemNanoMat* **2017**, *3*, 223.

[54] D. W. deQuilettes, S. Koch, S. Burke, R. K. Paranji, A. J. Shropshire, M. E. Ziffer, D. S. Ginger, *ACS Energy Lett.* **2016**, *1*, 438.

[55] K. P. Ong, T. W. Goh, Q. Xu, A. Huan, *J. Phys. Chem. A* **2015**, *119*, 11033.

[56] G. W. P. Adhyaksa, L. W. Veldhuizen, Y. Kuang, S. Brittman, R. E. I. Schropp, E. Garnett, *Chem. Mater.* **2016**, *28*, 5259.

[57] Y. Li, W. Yan, Y. Li, S. Wang, W. Wang, Z. Bian, L. Xiao, Q. Gong, *Sci. Rep.* **2015**, *5*, 14485.

[58] I. Levine, S. Gupta, T. M. Brenner, D. Azulay, O. Millo, G. Hodes, D. Cahen, I. Balberg, *J. Phys. Chem. Lett.* **2016**, *7*, 5219.

[59] W. Tian, C. Zhao, J. Leng, R. Cui, S. Jin, *J. Am. Chem. Soc.* **2015**, *137*, 12458.

[60] K. J. Williams, W. A. Tisdale, K. S. Leschkies, G. Haugstad, D. J. Norris, E. S. Aydil, X. Y. Zhu, *ACS Nano* **2009**, *3*, 1532.

[61] H. Li, D. Zhitomirsky, S. Dave, J. C. Grossman, *ACS Nano* **2016**, *10*, 606.

[62] K. Whitham, J. Yang, B. H. Savitzky, L. F. Kourkoutis, F. Wise, T. Hanrath, *Nat. Mater.* **2016**, *15*, 557.

[63] K. V. Reich, B. I. Shklovskii, *ACS Nano* **2016**, *10*, 10267.

[64] C. S. Ponseca, Y. Tian, V. Sundström, I. G. Scheblykin, *Nanotechnology* **2016**, *27*, 082001.

[65] W. J. Yin, T. Shi, Y. Yan, *Adv. Mater.* **2014**, *26*, 4653.

[66] A. Buin, R. Comin, J. Xu, A. H. Ip, E. H. Sargent, *Chem. Mater.* **2015**, *27*, 4405.

[67] W. S. Yang, B. W. Park, E. H. Jung, N. J. Jeon, Y. C. Kim, D. U. Lee, S. S. Shin, J. Seo, E. K. Kim, J. H. Noh, S. I. Seok, *Science* **2017**, *356*, 1376.

[68] C. Li, A. Guerrero, Y. Zhong, A. Gräser, C. A. M. Luna, J. Köhler, J. Bisquert, R. Hildner, S. Huettner, *Small* **2017**, *13*, 1701711.